Comparison of optical and conventional measurement techniques for experimental modal analysis of CFRP aero engine components

C. Schedlinski[1], K-H. Dufour[2], J. Schell[3], E. Biegler[3], J. Sauer[3], A. Hennig[1]

[1] ICS Engineering GmbH
  Am Lachengraben 5, 63303 Dreieich, Germany
  e-mail: **info@ics-engineering.com**

[2] Rolls-Royce Deutschland Ltd. & Co KG
  Eschenweg 11, 15827 Blankenfelde-Mahlow, Germany

[3] Polytec GmbH
  Polytec-Platz 1-7, 76337 Waldbronn, Germany

Abstract

Today, carbon fiber reinforced plastics (CFRP) are frequently used for light weight structure components of modern aero engines. In order to obtain reliable simulation results e.g. from Finite Element analyses, model validation of the related component models is mandatory and demands for highly accurate experimental data. Now, in this paper, different measurement scenarios for experimental modal analysis of CFRP aero engine structures will be applied to a typical CFRP structure. From the experiences made and the test results obtained the individual test scenarios will be evaluated and classified with respect to time, cost, and accuracy issues in order to provide guidance for choosing the optimal test setup for testing CFRP structures of aero engines especially with respect to the demands of subsequent model validation.

1   Introduction

Carbon fiber reinforced plastics (CFRP) are frequently used for light weight structure components of modern aero engines. Especially, they are essential to meet the overall mass requirements of the whole engine installation. Today, for example, intake, nacelle, and outlet are completely or at least partly built from CFRP parts.

To assist throughout the development and certification process, static and dynamic Finite Element (FE) analyses are conducted in order to assess the mechanical behavior of the aero engine. Because of the high degree of complexity of the utilized FE model, model validation based on computational model updating (see also [1]) is regularly employed at Rolls-Royce. A critical factor for success of the model validation campaign is a highly reliable experimental modal data base with the inherent demand for best practice measurement procedures.

In this paper, different measurement scenarios for experimental modal analysis (EMA) of CFRP aero engine structures shall therefore be evaluated. Especially, conventional accelerometer and optical laser measurements will be compared, while different test procedures as for instance hammer/shaker excitation or roving excitation/roving response measurements will be combined in order to perform multiple tests on a typical CFRP structure.

From the experiences made and the test results obtained the individual test scenarios will be evaluated and classified with respect to time, cost, and accuracy issues. Main goal is to give guidance for choosing the optimal test setup for testing CFRP structures of aero engines with respect to the demands of subsequent model validation.

2   Test item: thrust reverser door

The part to be investigated in the following is a door of a thrust reverser unit (TRU) of a contemporary Rolls-Royce aero engine. A survey of the TRU door is given in figure 1. In principle the door consists of CFRP panels and ribs interconnected by rivets.

Figure 1: Survey of TRU door, left: outer, right inner view

3   Survey of tests to be conducted

In order to assess the advantages and disadvantages of today's most commonly employed test procedures, the following tests are to be conducted for the TRU door:

1. Acceleration measurements
   o shaker excitation
     ▪ nonlinearity investigation
     ▪ stinger/force sensor attachment influence investigation
     ▪ mass loading investigation
     ▪ (roving accelerometer) modal test
   o hammer excitation
     ▪ roving hammer modal test
     ▪ roving accelerometer modal test
2. Scanning Laser Doppler Vibrometer (SLDV) measurements
   o shaker excitation
     ▪ roving laser modal test

Especially, principle investigations are undertaken with shaker excitation and accelerometer measurements at first in order to assess potential influences due to nonlinearities (CFRP material, rivet connections, etc.) and test procedure itself (shaker attachment, sensor influence).

4   Test planning

Before testing, dedicated test planning is conducted. Test planning thereby utilizes a Finite Element (FE) model, and enables not only the test design but also considerably simplifies the later correlation with the analytical results (Finite Element model and test model 'match'). Test planning should cover the following aspects:

- definition of boundary conditions

- selection of relevant target modes

- selection of measurement degrees of freedom with respect to
    - essential test information
    - sufficient spatial resolution of the target modes (linear independence)
    - coincidence of measurement and FE model nodes
    - accessibility of the measurement nodes
    - redundancy of the measurement degrees of freedom
    - robustness of the test model

- selection of exciter positions (if possible, simultaneous excitation of all target modes)

- sufficient frequency resolution (for proper identification of modal data)

At ICS test planning is conducted utilizing a special Matlab based software package (ICS.sysval, [2]), which was also developed by ICS. Particularly for the TRU door, the following targets were defined before test planning and development of the test models (measurement nodes, measurement directions and wire frame):

- free/free boundary conditions

- frequency range 0…~600 Hz (first 50 elastic modes)

Main goal is to provide best possible test models and a priori test setup specifications in order to obtain highly reliable test data.

4.1   Test planning results

Test planning was based on an existing FE model of the TRU door.

The test models derived for conventional accelerometer measurements and for laser (SLDV) measurements are presented in figure 2. A total of 74 (conventional) and 629 (laser) measurement nodes were defined and local measurement coordinate system normal to the panel surfaces were introduced for conventional measurements in order to allow for hammer excitation/sensor application normal to the panels (no adapters required to align with global Cartesian coordinate system).

The results of an analytical modal analysis with the test models coupled to the FE model, serve as the basis for the validation of the test models. Auto-MAC matrices (MAC of analytical modes versus themselves) are calculated, considering only the selected measurement degrees of freedom (i.e. only a subset). Figure 3 shows these Auto-MAC matrices and it can be seen that the individual analytical mode shapes are very well decoupled (practically diagonal form of Auto-MAC matrix) for the laser test model only, allowing to uniquely pair test and analytical mode shapes by subsequent test/analysis correlation procedures. For the conventional test model, however, selected off-diagonal terms are found indicating spatial aliasing (some mode shapes 'look alike' at the selected measurement degrees of freedom). The corresponding modes are highly local panel modes that are not considered relevant; to that extend the test model is acceptable as well.
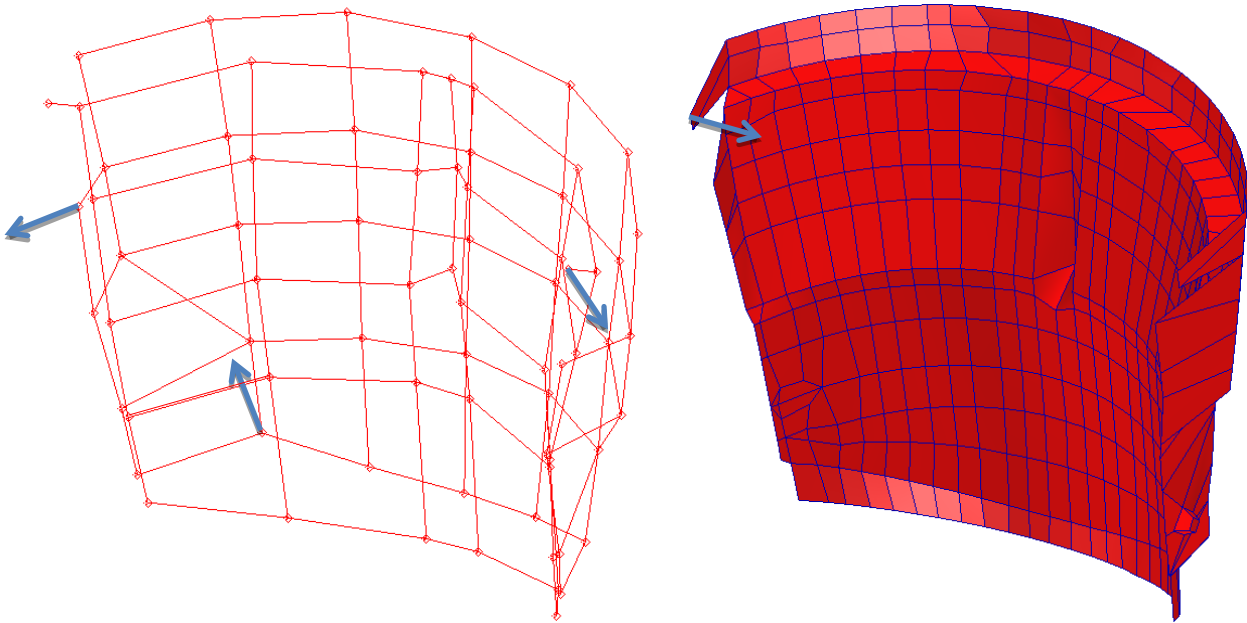
Figure 2: Test model for left: conventional and right: laser measurements
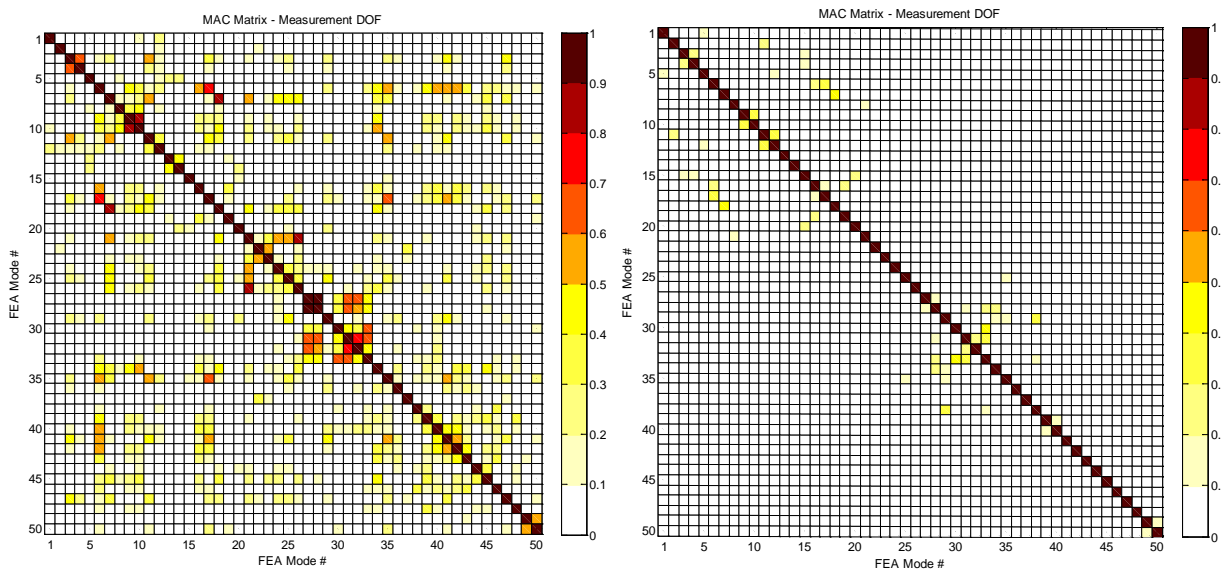(planned excitation directions marked as arrows)

Figure 3: Auto-MAC Matrix for left: conventional and right: laser measurements

To identify appropriate excitation directions, mode indicator functions (MIF) are calculated. For a given excitation direction and mode shape pair a MIF value of zero indicates perfect excitation of the mode shape (fulfillment of phase resonance criterion), a value of one indicates no excitation at all. For the TRU door excitation directions were selected according to figure 2, and the corresponding MIF values are shown in figure 4 (2% modal damping assumed for calculation). It can be seen that an acceptable level of excitation of practically all target mode shapes can be realized for the conventional measurements ('lightly-colored' path through MIF values). For the laser measurements some modes cannot be excited well enough by the selected exciter position. Nevertheless, this is accepted due to accessibility and attachment requirements and for the sake of keeping testing time within reasonable limits (only one excitation configuration).
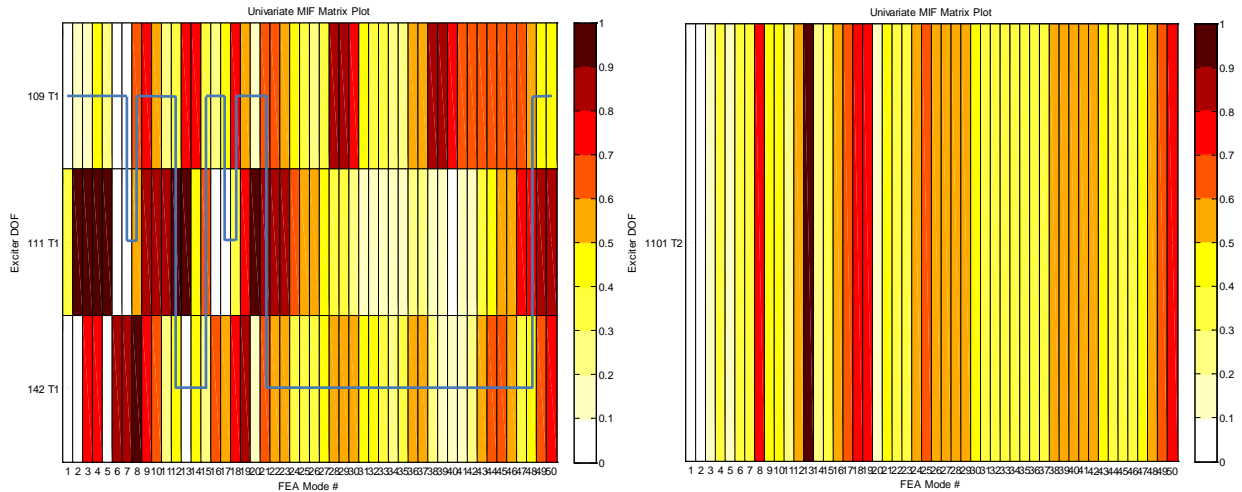
Figure 4: MIF values for selected excitation directions for left: conventional and right: laser measurements

4.2   Ideal versus real test model

A typical difficulty for conventional modal testing is that the ideal measurement locations according to the test plan need to be marked on the real hardware. Now, for curved panel like surfaces without clear reference points or with geometric differences to the model this can be a challenging task.

To check the influence of possible misalignments of ideal versus real test model, the marked test nodes for the conventional test model were digitalized again by sonic triangulation, see figure 5. The digitization shows misalignments with respect to the mean overall dimension of the TRU door from about 0.2% to 6% with a mean of about 2%. The rather high outliers of up to about 6% can be attributed to the fact, that the FE model used for test planning exhibits some geometric simplifications that differ (in some cases significantly) from the real hardware.

Figure 5: Setup for digitization

The effects of this misalignment are demonstrated with the help of the FE model. An analysis with ideal and with real test model attached to the FE model is made, and a subsequent correlation based on normal measurement degrees of freedom only is performed between the two models. The MAC matrix from this exercise is shown in figure 6 for the first 10 elastic modes. It can be noted that significant bias occurs due to the geometric misalignment. Thus, for further processing, the digitized test model must be used in any case.
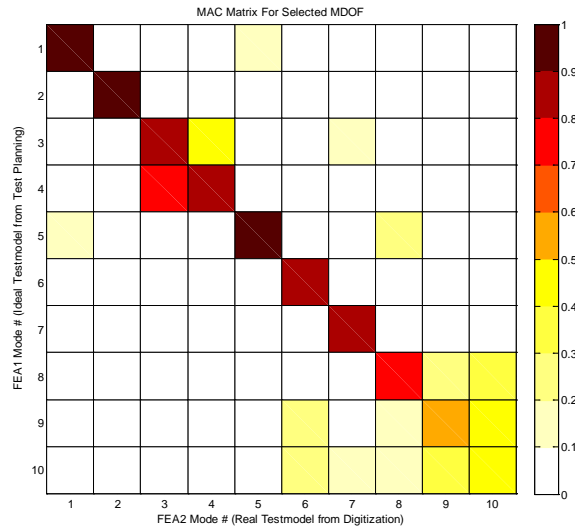

Figure 6: MAC Matrix ideal versus real test model

5 Principle investigations

5.1 Nonlinearity

To assess the degree of nonlinearity, a dedicated study is done based on step sine shaker measurements with controlled excitation force. In detail, several force levels are applied and held constant within 3% limit. Figure 7 shows the controlled force levels 0.05 N, 0.5 N, and 4 N (see right side of figure 2 above for excitation location); figure 8 the corresponding reference frequency response functions (FRFs). The overall level of nonlinearity is rather low, only a slight increase of damping and decrease of resonance frequency is observed for selected resonances. Thus nonlinearity will not have a significant impact on subsequent modal testing.
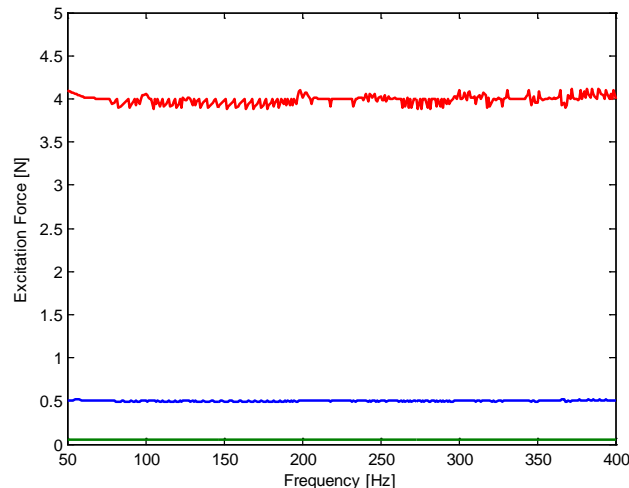

Figure 7: Controlled excitation forces, green: 0.05 N, blue: 0,5 N, red: 4 N excitation force
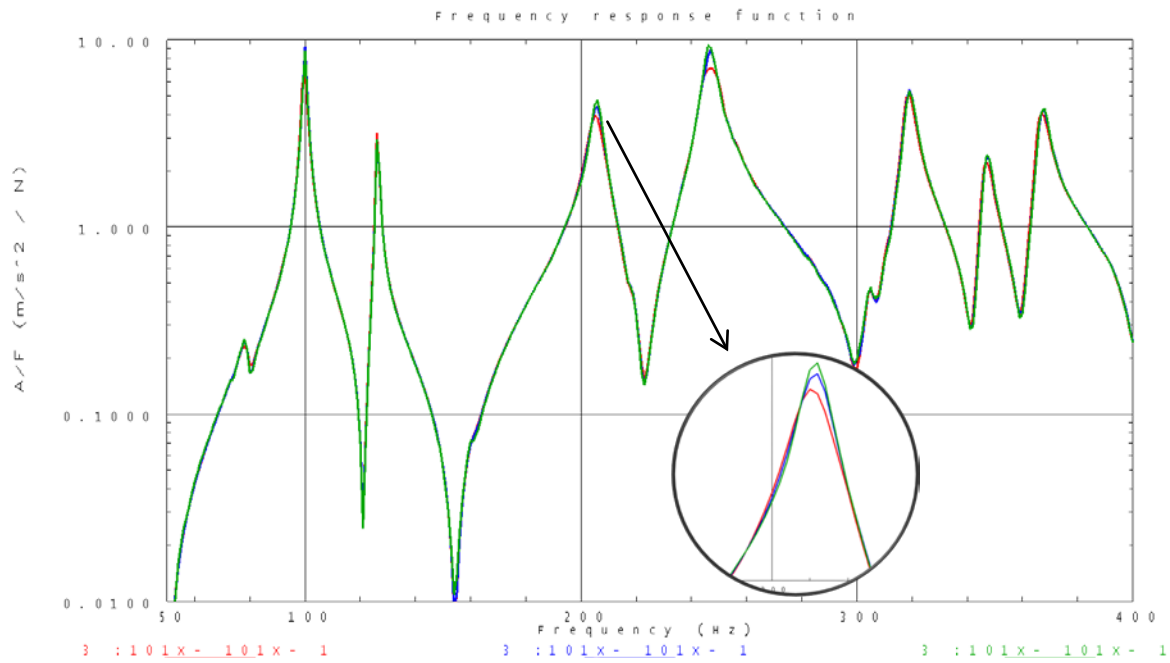
Figure 8: Typical FRFs, green: 0.05 N, blue: 0,5 N, red: 4 N excitation force

5.2   Stinger/force sensor attachment

To assess the influence of stinger and force sensor attachment to the test item three different configurations are compared:

1. Hammer excitation without stinger and without force sensor (figure 9, left)

2. Hammer excitation without stinger and with force sensor (figure 9, mid)

3. Shaker excitation with stinger and with force sensor (figure 9, right)

Figure 10 shows the reference FRFs for configurations 1 and 2; figure 11 shows the reference FRFs for configurations 2 and 3. The attachment of the force sensor leads to amplitude changes for some resonance frequencies while the effect is more pronounced in the upper frequency range. The resonance frequencies are practically not changed. The selected stinger (nylon stinger with rather high flexibility and high internal damping) does not significantly change the dynamics of the system. All in one the complete stinger/force sensor attachment does not significantly alter the system behavior.

Figure 9: Configurations for stinger/force sensor attachment investigation
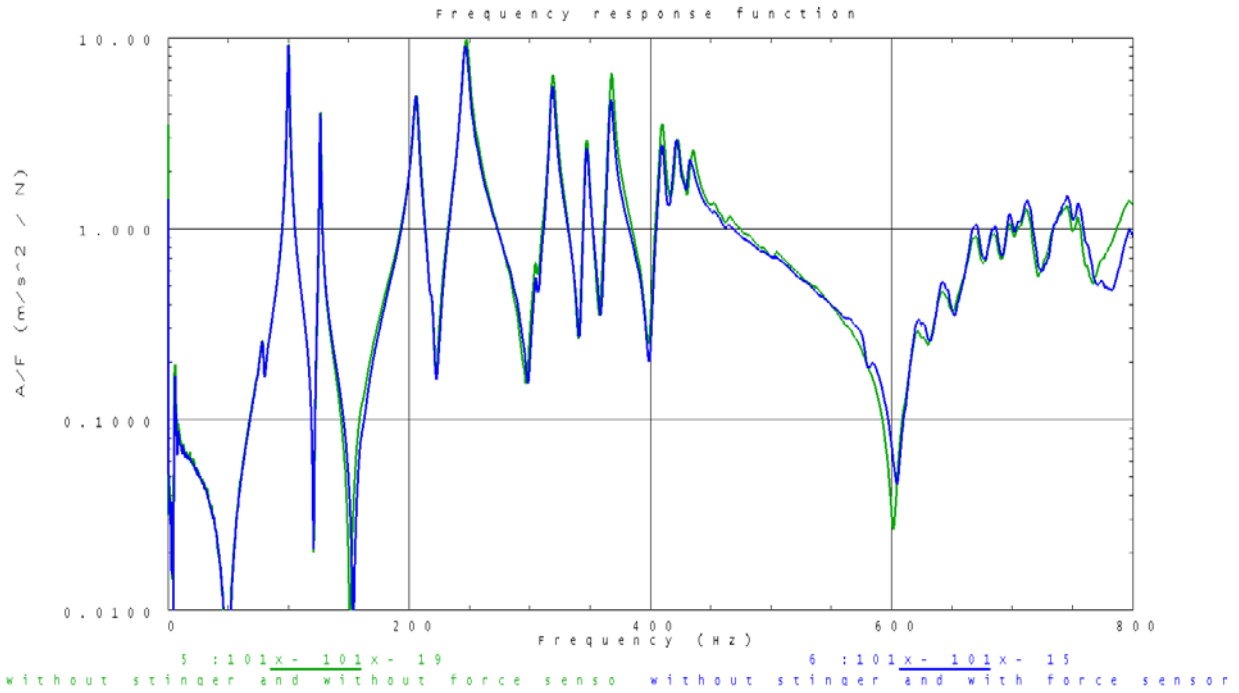
Figure 10: Reference FRF without and with force sensor (without stinger)
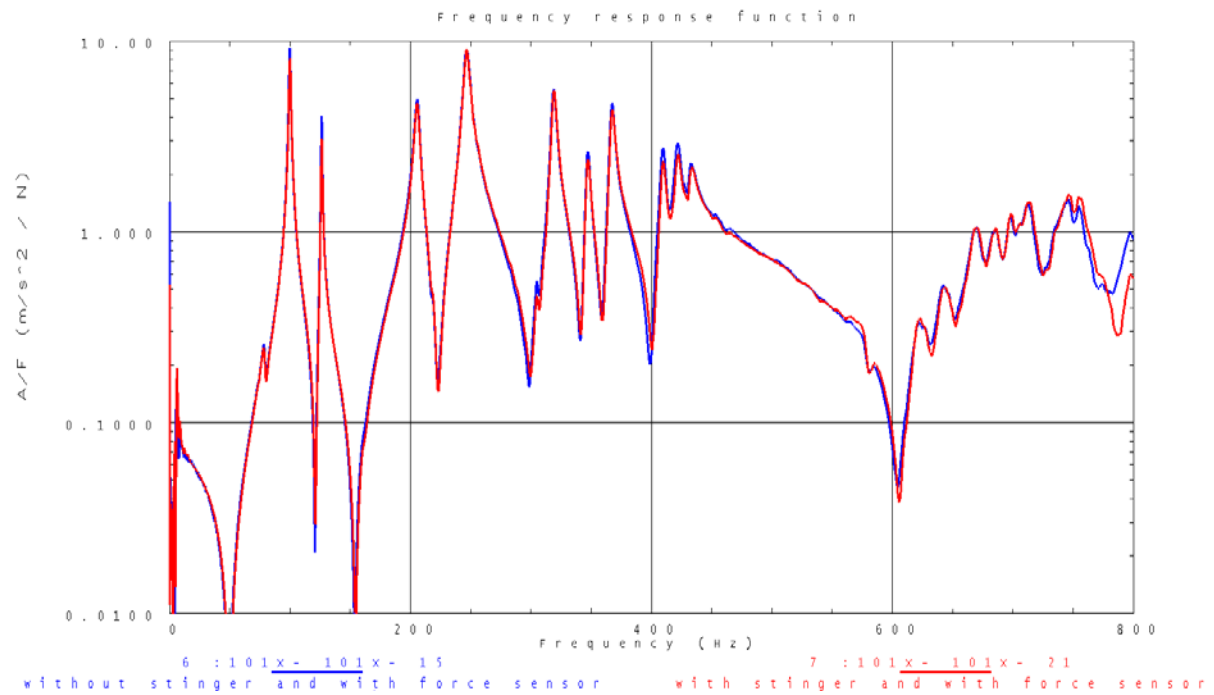
Figure 11: Reference FRF without and with stinger (with force sensor)

5.3 Mass loading

A last investigation is focused on mass loading. The motivation is to assess the change in dynamic behavior of the TRU door due to moving masses of sensors during roving accelerometer tests. Three configurations were measured for one set off accelerometers attached to the TRU door: 1st sensors alone, 2nd sensors plus one additional dummy mass per sensor, and 3rd sensors plus two additional dummy mass per sensor. Figure 12 highlights the three configurations for one exemplary sensor.

Figure 12: Mass loading setup

Figure 13 shows the corresponding FRFs for the reference location and the sensor shown in figure 12 (which was more or less mounted in the middle of a free panel section). Up two about 400 Hz practically no impact on the behavior of the system can be noted. Above 400 Hz (more localized modes), mostly amplitudes and –in some cases – also resonance frequencies are affected by the additional masses. Since the amplitude changes are not consistent for both measured locations, the effect can rather be attributed to the change in mass than to a change in damping.
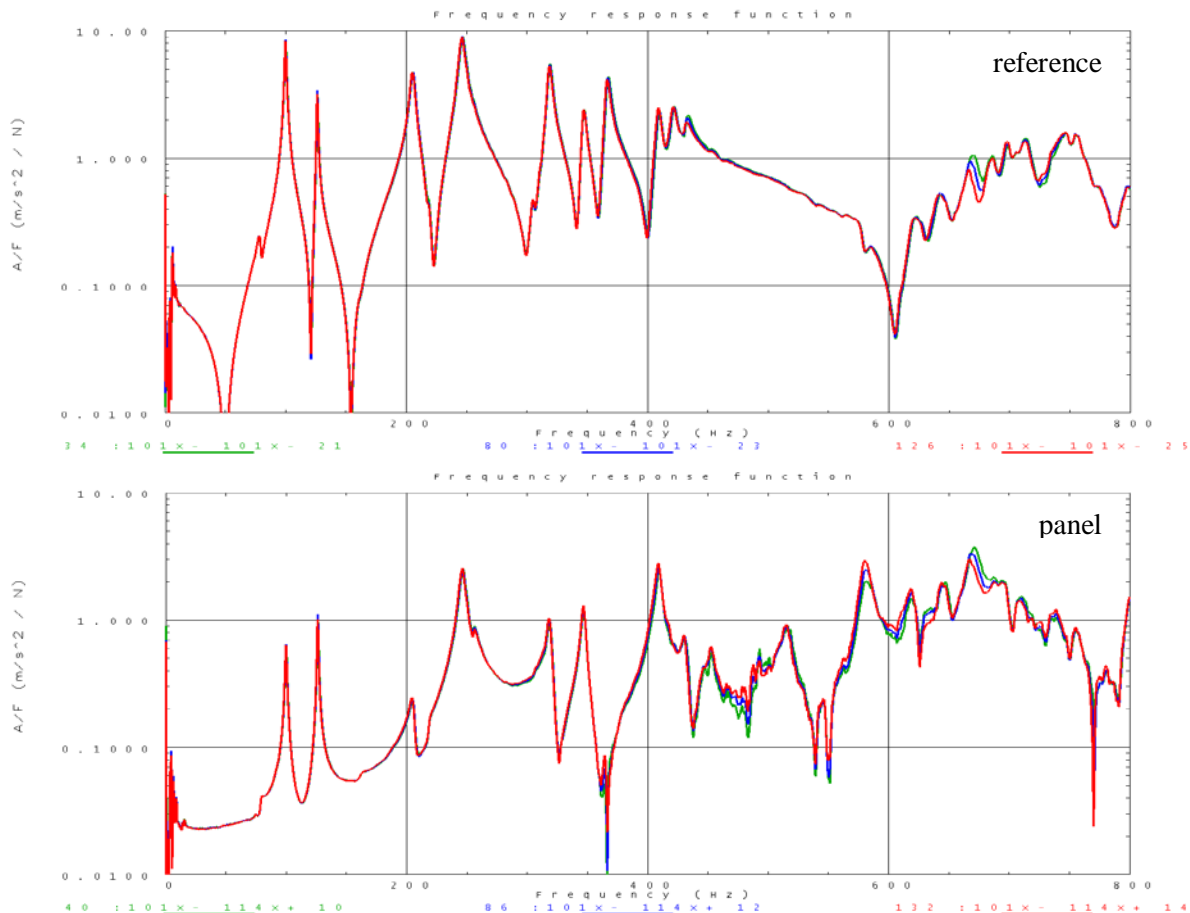

Figure 13: Upper plot: reference FRF, lower plot: panel FRF
green: sensor only, blue: with one additional mass, red: with two additional masses

6   Experimental modal analysis

In this section the results from four different tests conducted for EMA are presented, namely roving acceleration measurements with fixed shaker and hammer excitation, roving hammer excitation with fixed acceleration measurements, and roving laser measurements (automated 3D laser scanner – RoboVib, [3-4]) with shaker excitation. Table 1 summarizes the main settings of the individual tests; figure 14 shows two typical setups. For all tests the TRU door was resiliently suspended by elastomer cords.

Test ID	RvA-S	RvA-H	RvH	RvL-S
Test Type	Roving Acceleration	Roving Acceleration	Roving Hammer	Roving Laser
Excitation Signal	Shaker/Random	Hammer Impact	Hammer Impact	Shaker/Pseudo Random
Response Signal	Acceleration (triaxial)	Acceleration (triaxial)	Acceleration (uniaxial)	Laser Scanner (RoboVib)
Frequency Range [Hz]	0…1600	0 … 3200	0 … 3200	10…800
Frequency Resolution [Hz]	0.25	0.5	0.5	0.5
Number of Spectral Lines	6401	6401	6401	1581
Averaging Frames	50	7	7	10
Window Function	Hanning	Exponential Decay	Exponential Decay	none
Number of Measurement DOF	222 (74 triaxial)	99 (33 triaxial)	74 (normal to surface)	2319 (773 triaxial)
Number of References	1	3	3	1

Table 1: Main settings of the individual tests

Figure 14: Typical test setup, left: conventional hammer test, right: automated 3D laser scanner (RoboVib)

Now, for every test FRFs were estimated from the measured quantities. Figure 15 exemplarily shows the imaginary parts of all FRFs for roving acceleration measurements with fixed shaker excitation (RvA-S). Clear and pronounced resonance peaks can be found up to about 450-500 Hz. Above, modal density increases significantly which effectively complicates modal data extraction in the upper frequency range.
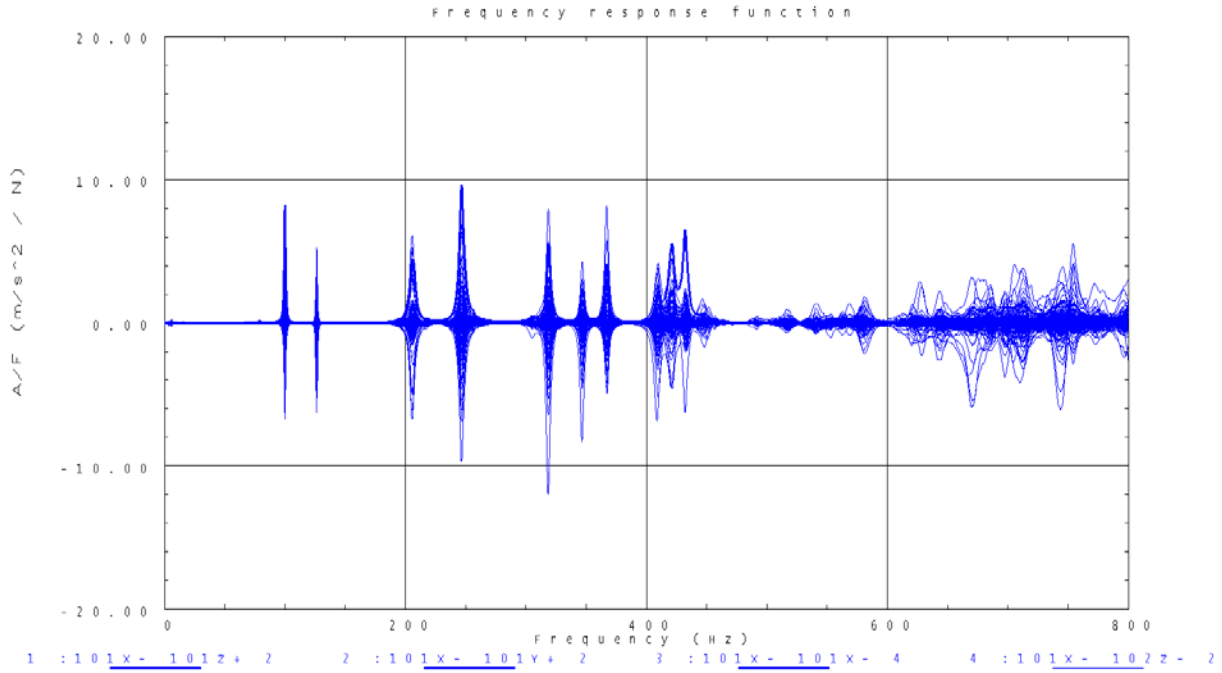
Figure 15: All FRFs for test RvA-S (imaginary parts only)

Modal data was therefore identified only up to 500 Hz for all tests. MIF calculations based on the measured FRFs indicate 22 resonances in this frequency range (see also figure 16). Table 2 shows the results for the four tests. Resonances marked orange or red could only be identified with less to poor confidence from the corresponding tests.

No.	RvA-S		RvA-H		RvH		RvL-S	
	Freq. [Hz]	Modal Da. [%]	Freq. [Hz]	Modal Da. [%]	Freq. [Hz]	Modal Da. [%]	Freq. [Hz]	Modal Da. [%]
1	99.95	0.66	100.02	0.77	100.02	0.77	99.57	0.68
2	126.31	0.33	126.57	0.28	126.57	0.28	126.40	0.29
3	205.71	1.21	205.17	1.03	205.17	1.03	199.71	2.02
4	246.73	1.01	247.71	1.14	247.71	1.14	248.05	1.44
5	256.04	0.71	255.43	0.71	255.43	0.71	255.82	0.59
6	304.94	0.79	304.67	0.79	304.67	0.79	304.28	0.77
7	312.79	1.85	313.70	0.75	313.70	0.75	312.81	0.79
8	318.56	0.63	319.59	0.63	319.59	0.63	319.14	0.63
9	327.87	0.69	327.65	0.66	327.65	0.66	327.84	0.59
10	346.76	0.53	346.50	0.53	346.50	0.53	346.90	0.52
11	367.12	0.53	367.56	0.57	367.56	0.57	367.37	0.53
12	409.38	0.53	409.72	0.72	409.72	0.72	409.63	0.64
13	421.53	0.63	421.33	0.79	421.33	0.79	420.68	0.76
14	432.09	0.54	434.18	0.65	434.18	0.65	432.54	0.55
15	447.87	0.91	446.90	0.88	446.90	0.88	448.00	0.84
16	-	-	450.42	0.42	450.42	0.42	-	-
17	451.91	0.78	451.89	0.59	451.89	0.59	451.82	0.66
18	-	-	457.83	0.41	457.83	0.41	457.32	0.51
19	461.22	0.98	464.36	0.66	464.36	0.66	464.77	1.06
20	471.70	0.53	471.46	0.69	471.46	0.69	-	-
21	-	-	480.33	0.67	480.33	0.67	-	-
22	491.81	0.42	491.52	0.59	491.52	0.59	491.67	0.70

Table 2: EMA results of four individual tests

The main reason for the poor confidence ratings of the shaker tests is the fact that only one reference is available here, and the related resonances are not excited very well by this very reference. To illustrate this further the multivariate MIF of the roving hammer test calculated from all three references is superimposed in figure 16 by the standard MIF of the roving accelerometer test with shaker excitation. Comparing the marked frequencies from table 2 with the MIFs from figure 16 directly shows relatively poor MIF value indicating less good excitation. Thus, for further comparison of the tests, the resonances with poor confidence ratings will be omitted.
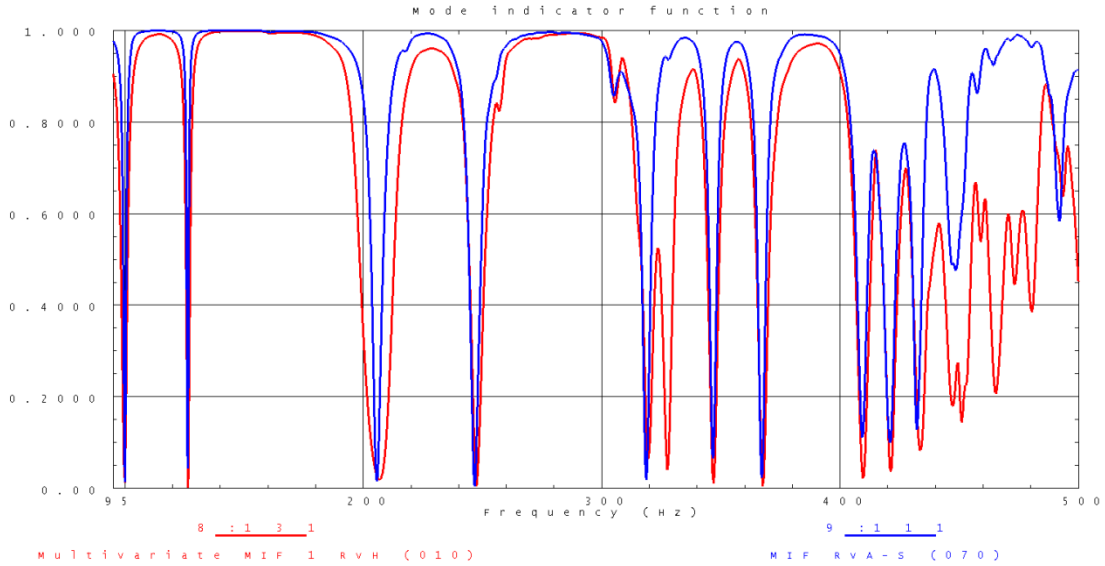

Figure 16: Typical MIF curves

Exemplarily, tables 3 and 4 show correlations of the roving hammer test versus the roving accelerometer test with hammer excitation as well as of the roving accelerometer test with hammer excitation versus the roving accelerometer test with shaker excitation.

#	EMA1	EMA2	EMA1 [Hz]	EMA2 [Hz]	Dev. [%]	MAC [%]
1	1	1	100.02	99.89	−0.13	99.94
2	2	2	126.57	126.50	−0.06	99.90
3	3	3	205.17	211.51	3.09	98.32
4	4	4	247.71	247.29	−0.17	99.92
5	5	5	255.43	257.24	0.71	99.81
6	6	6	304.67	305.44	0.25	99.81
7	7	7	313.70	315.14	0.46	94.66
8	8	8	319.59	319.39	−0.06	99.29
9	9	9	327.65	327.78	0.04	99.73
10	10	10	346.50	347.00	0.14	99.88
11	11	11	367.56	367.54	−0.00	99.76
12	12	12	409.72	409.68	−0.01	99.79
13	13	13	421.33	421.36	0.01	99.22
14	14	14	434.18	434.16	−0.00	99.39
15	15	15	446.90	447.30	0.09	98.93
16	16	16	450.42	451.21	0.18	85.04
17	17	17	451.88	453.01	0.25	85.82
18	18	18	457.83	459.08	0.27	97.84
19	19	19	464.36	464.76	0.09	94.86
20	20	20	471.46	473.32	0.39	83.05
21	21	21	480.33	480.85	0.11	96.13

Table 3: Correlation EMA1: RvH versus EMA2: RvA-H

```
 #    EMA1   EMA2   EMA1 [Hz]   EMA2 [Hz]   Dev. [%]   MAC [%]
 1     1      1      100.02       99.95      -0.06      99.30
 2     2      2      126.57      126.31      -0.21      94.08
 3     3      3      205.17      205.71       0.26      97.46
 4     4      4      247.71      246.73      -0.40      98.58
 6     6      -
 8     8      8      319.59      318.56      -0.32      92.66
10    10     10      346.50      346.76       0.07      99.15
11    11     11      367.56      367.12      -0.12      97.11
12    12     12      409.72      409.38      -0.08      89.18
13    13     13      421.33      421.53       0.05      90.88
14    14     14      434.18      432.08      -0.48      73.93
15    15     15      446.90      447.87       0.22      80.38
```

Table 4: Correlation EMA1: RvA-H versus EMA2: RvA-S

The first correlation in table 3 highlights that no significant differences between roving hammer and roving accelerometer tests are present. This is in line with the observations made during the principle investigations. Thus, the TRU door system in general does not behave too sensitive with respect to mass loading effects. The second correlation in table 4 exhibits slightly higher differences in the upper frequency range with respect to MAC correlation of the mode shapes that can be assigned to the effects of the mounted force sensor for shaker excitation.

All in one the results from the four different testing techniques are rather consistent, as long as a sufficient excitation level of the resonances can be achieved, and no adverse effects can be attributed to the CFRP design of the TRU door.

7   Comparison of test procedures

Finally table 5 summarizes the advantages and disadvantages of the four applied test procedures which – if conducted thoroughly – will yield EMA data of comparable quality.

Feature	RvA-S	RvA-H	RvH	RvL-S
General Features				
overall costs (time/equipment)	medium to high	medium to high	Low	High
setup/rigging time	medium to high	medium to high	Low	Medium
testing time	low to high [1]	low to high [1]	medium to high	medium to high
preparation of test item required	no	no	No	no/yes [2]
automated measurement	no	no	No	Yes
realistically achievable spatial resolution	medium to high	medium to high	medium to high	very high
Interference with measurement object				
mass loading, response	yes	no	Yes	No
mass loading, excitation force	yes	no	No	Yes
possible stinger influence	yes	no	No	Yes
Data features and nonlinearity				
overall signal to noise ratio	highest	medium to high	low to high	medium to high
suitability for nonlinear systems [3]	yes	limited	No	Yes

[1] depending on available channel count   [2] for poor reflective properties   [3] linearization by control of excitation force level

Table 5: Comparison of test procedures

8   Summary and conclusions

For the TRU door made from CFRP different measurement scenarios for EMA were evaluated in order to assess their principle capabilities and restrictions. Especially, conventional accelerometer and optical laser measurements were compared, while different test procedures as for instance hammer/shaker excitation or roving excitation/roving response measurements were combined.

First investigations showed that the TRU door does not exhibit significant nonlinearity and is not too sensitive to mass loading due to roving accelerometers. In the end, all applied methods provided EMA data of comparable quality. However, it showed as well that sufficient excitation of all target modes is mandatory in order to obtain reliable EMA data and must be ensured by thorough test planning in advance.

As a basic guideline it can be said that conventional tests are fine in case of moderate spatial resolution of the test model. If a very high resolution of the test model is required (e.g. for visualization of local effects) the automated laser measurement is in favor.

In case of nonlinearities the application of roving hammer testing is strongly limited. Here, shaker excitation offers clear advantages to hammer excitation because of the capability to fully control the input force and thus linearize the system during the test. However, mass loading due to (e.g.) accelerometers may become a critical issue especially when measuring structural parts with low seismic mass (for instance thin panels). Here, either special lightweight sensors or laser measurements must be applied.

It has proven to be good practice to assess nonlinear behavior and the disposition for mass loading effects at first (e.g. by simple hammer pretests) in order to define the proper test technique before conducting the final test.

Acknowledgment

References

[1] M. Böswald, M. Link, C. Schedlinski, *Computational Model Updating and Validation of Aero-engine Finite Element Models Based on Vibration Test Data*, IFASD 2005, Munich, (2005)

[2] C. Schedlinski, *ICS.sysval product description*, ICS homepage http://www.ics-engineering.com, (2014).

[3] M. Johansmann; J. Sauer, *A New Tool for Three Dimensional Non-contact Vibration Measurements in Automotive Applications*, SAE Paper No. 2005-26-052, (2005).

[4] M. Schüssler, D. E. Oliver, *Fully Automated Robot-based 3-Dimensional Vibration Measurement System for Modal Analysis and Structural Health Monitoring*, Proceedings of the IMAC-XXVII, (2009).